Electrochemistry Communications 108 (2019) 106556

Contents lists available at ScienceDirect

Electrochemistry Communications

journal homepage: www.elsevier.com/locate/elecom

Short Communication

Avidin-gated mesoporous silica nanoparticles for signal amplification in electrochemical biosensor

Sandra Jimenez-Falcao[a], Jorge Parra-Nieto[a], Hugo Pérez-Cuadrado[a], Ramón Martínez-Máñez[b,c,d,e], Paloma Martínez-Ruiz[a,*], Reynaldo Villalonga[a,*]

[a] Nanosensors and Nanomachines Group, Department of Analytical Chemistry, Faculty of Chemistry, Complutense University of Madrid, 28040 Madrid, Spain
[b] Instituto Interuniversitario de Investigación de Reconocimiento Molecular y Desarrollo Tecnológico (IDM), Universitat Politècnica de València, Universitat de València, Camino de Vera s/n, 46022 Valencia, Spain
[c] Unidad Mixta UPV-CIPF de Investigación en Mecanismos de Enfermedades y Nanomedicina, Universitat Politècnica de València, Centro de Investigación Príncipe Felipe, Valencia, Spain
[d] Unidad Mixta de Investigación en Nanomedicina y Sensores. Universitat Politècnica de València, IIS La Fe, Valencia, Spain
[e] CIBER de Bioingeniería, Biomateriales y Nanomedicina (CIBER-BBN), Spain

ARTICLE INFO

Keywords:
Aptamer
Biosensor
Carcinoembryonic antigen
Mesoporous silica nanoparticles
Signal amplification

ABSTRACT

We report herein a novel sensing strategy for electrochemical biosensors, by using mesoporous silica nanoparticles loaded with the redox probe methylene blue and capped with an avidin/imminobiotin stimulus-responsive gate-like ensemble as signal amplification element. As a proof of concept, an aptasensor for carcinoembryonic antigen (CEA) was constructed by attaching a biotin and thiol-functionalized anti-CEA DNA hairpin aptamer on gold nanoparticles modified carbon screen-printed electrodes. The biosensing approach relied on the unfolding of the aptamer molecule after specific recognition of CEA, unmasking the biotin residue and allowing further association with the avidin-capped mesoporous nanocarrier. Incubation with H_2SO_4 trigger the release of the encapsulated redox probe allowing the detection of the cancer biomarker from 1.0 pg/mL to 160 ng/mL.

1. Introduction

The development of new amplification strategies for affinity-based electrochemical biosensors receives considerable attention to allow construction of more sensitive analytical devices [1,2]. Current amplification approaches are mainly based on enzymes-catalyzed reactions [3–5], but novel enzyme-free amplification methods are desired to confer robustness, reproducibility and stability to bioelectroanalytical sensors [6,7]. In fact, enzyme are labile globular proteins that progressively loose catalytic activity if not stored in proper conditions, thus affecting the reliability of the resulting biosensor. Enzymes are also relatively expensive, and their substitution should improve the price-effectiveness of the resulting biosensors.

Nanomaterials have been largely explored to label antibodies, aptamers and other nucleic acid molecules for electrochemical biosensors construction [8]. They have been also employed as scaffold to successful assemble original amplification units [1,2]. In this context, mesoporous silica nanoparticles (MSN) offer unique advantages as amplification elements due to their high load capacity for redox probes, easy preparation with controlled morphology, size and pore diameter, and facility to be mechanized with stimulus-responsive gate-like ensembles allowing on-command release of the cargo [9].

Here we describe, for the first time, the preparation of a MSN nanocarrier loaded with methylene blue (MB) as redox probe and functionalized with a pH-sensitive avidin/iminobiotin ensemble acting as biomolecular gatekeeper and biotin-recognition unit. As a proof-of-concept, this nanodevice was employed to amplify the detection of carcinoembryonic antigen (CEA), a relevant cancer biomarker [10]. In this regard, an electrochemical aptasensor was constructed by using a biotin and thiol-modified anti-CEA DNA hairpin aptamer as bioreceptor, and carbon screen-printed electrodes modified with gold nanoparticles (AuNP/SPE) as transduction interface.

2. Materials and methods

2.1. Reagents and instruments

All reagents and solvents were from Sigma-Aldrich (USA). AuNP/

* Corresponding authors.
E-mail addresses: palmarti@ucm.es (P. Martínez-Ruiz), rvillalonga@quim.ucm.es (R. Villalonga).

https://doi.org/10.1016/j.elecom.2019.106556
Received 3 August 2019; Received in revised form 15 September 2019; Accepted 16 September 2019
Available online 04 October 2019

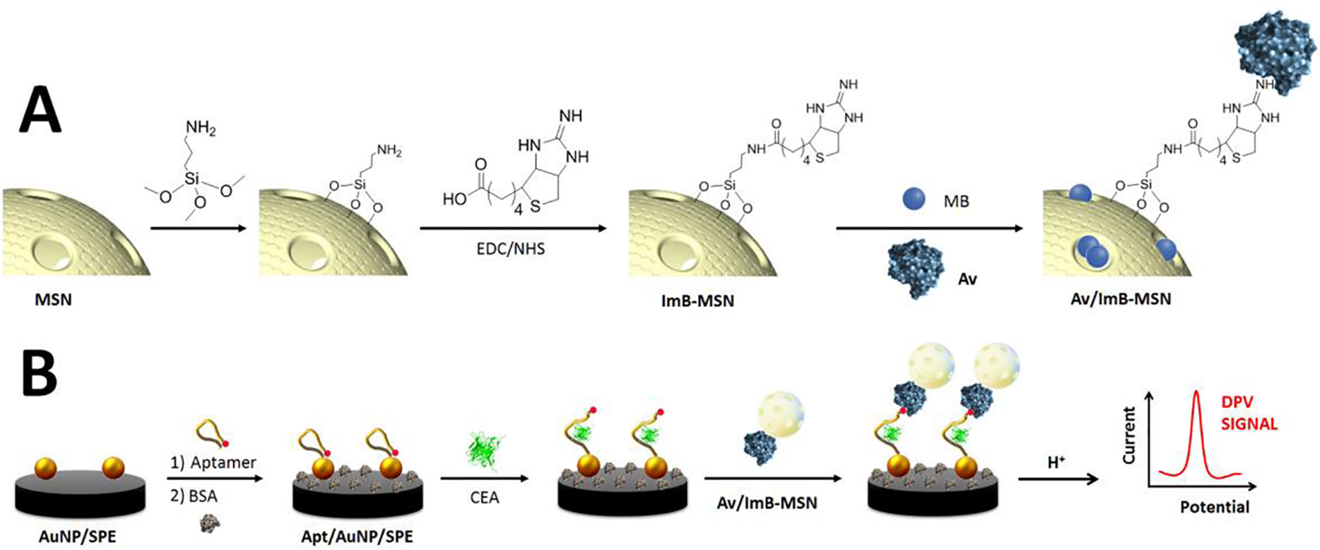

Fig. 1. Schematic display of the processes involved in the preparation of the Av/ImB-MSN nanocarrier (A) and the construction and use of the aptasensor for CEA determination (B).

SPE were purchased from Orion High Technologies (Spain, www.orion-hitech.com) and used as received. The anti-CEA aptamer modified with thiol and biotin groups at the 5′ and 3′ ends, respectively (5′-HS-$(CH_2)_6$-CCAC GATA CCAG CTTA TTCA ATTC GTGG-biotin-3′ [11]) was acquired from Sigma-Aldrich (USA).

Electrochemical measurements were performed with a PalmSens4 potentiostat (PalmSens BV, The Netherlands, www.palmsens.com). Transmission electron microscopy (TEM) measurements were carried out with a JEOL JEM-2100 microscope (JEOL Ltd., Japan). Spectrophotometric measurements were performed with an Ultrospec™ 8000 Dual Beam UV/VIS spectrophotometer (Biochrom™, UK). FT-IR spectra were recorded on a Perkin Elmer Spectrum 400 Series spectrometer (Perkin Elmer, USA). Powder X-ray diffraction (XRD) was performed with an X'Pert MRD diffractometer (PANanalytical B.V., The Netherlands). Nitrogen adsorption/desorption isotherms and pore size distributions were determined with an ASAP 2020 Physisorption Analyzer (Micromeritics, USA). Thermal analysis was performed with a TA Instruments SDT-Q600 apparatus (USA).

2.2. Preparation of MSN-based amplification element

MSN was first prepared as previously described [12], and then functionalized with primary amino groups by dispersing 50 mg MSN in 2.0 mL toluene under sonication and mixed with 50 μL (3-aminopropyl) triethoxysilane. The mixture was stirred at room temperature during 24 h, then filtered, washed with toluene and dry at 60 °C. 25 mg of amino-functionalized MSN were dispersed in 2.0 mL of cold 0.1 M sodium phosphate buffer, pH 8.5, and mixed with 50 μL of 0.1 M HCl solution containing 27 mg 2-iminobiotin. The mixture was stirred at 4 °C and then 27 mg 1-ethyl-3-(3-dimethylaminopropyl)carbodiimide hydrochloride and 11 mg N-hydroxysuccinimide were added. The mixture was stirred for 24 h at 4 °C, and the resulting solid (ImB-MSN) was centrifuged, washed three times with 0.1 M sodium phosphate buffer, pH 7.0, and further dispersed in 2.0 mL of the same buffer containing 5 mg MB. The mixture was stirred for 24 h at 4 °C to load the redox probe into the MSN face pores and then 5.0 mg avidin were added. After 24 h at 4 °C under continuous stirring, the final blue solid (Av/ImB-MSN) was centrifuged and exhaustively washed with the same cold buffer until not MB was detected in the washing solution. The solid was redispersed in 0.1 M sodium phosphate buffer, pH 7.0, at 5 mg/mL final concentration and kept at 4 °C until use.

2.3. Preparation of aptamer-functionalized electrodes (Apt/AuNP/SPE)

Firstly, to fold the aptamer to the hairpin structure, 20 μL of 100 μM anti-CEA aptamer solution were mixed with 80 μL of 100 mM NaCl, 5 mM $MgCl_2$ in 20 mM Tris-HCl buffer solution, pH 7.40, heated at 95 °C during 5 min followed by slow cooling to room temperature. The aptamer solution was then mixed with 100 μL of 8 mM tris(2-carboxyethyl)phosphine hydrochloride and 8 μL of folded aptamer (final concentration, 7 μM) were dropped on the working electrode surface. After 20 min of incubation at room temperature, the electrode was washed with milliQ water, dried under N_2 and then 8 μL of 2% (w/v) BSA solution in 0.1 M sodium phosphate buffer, pH 7.4 were dropped on the electrode surface. After 40 min incubation at 4 °C, the Apt/AuNP/SPE electrode was exhaustively washed with 0.1 M sodium phosphate buffer, pH 7.4, dried under N_2 and kept at 4 °C until use.

2.4. Electroanalytical procedure

CEA samples were prepared in 0.1 M sodium phosphate buffer, pH 7.4, and 8 μL were dropped on the Apt/AuNP/SPE surface and kept at room temperature during 20 min in a humid chamber. The electrode was then washed with buffer, dried under N_2, and 8 μL of 0.5 mg/mL Av/ImB-MSN dispersion in the same buffer were dropped on the working electrode surface. After 20 min incubation at room temperature, the electrode was washed and dried, and then 80 μL of 0.5 M H_2SO_4 were added to the electrochemical cell. Differential pulse voltammetry measurements were finally performed after 5 min incubation in the acid solution.

3. Results and discussion

The steps involved in the preparation of the Av/ImB-MSN nanocarrier are shown in Fig. 1A. MSN, previously modified with (3-aminopropyl)triethoxysilane, were functionalized with 2-iminobiotin and then loaded with MB as redox probe for electrochemical signal amplification. These nanoparticles were finally capped with avidin though affinity interactions with the 2-iminobiotin residues. The rational of using 2-iminobiotin to construct this nanocarrier was based on the lower affinity of avidin for this derivative in comparison with biotin [13], allowing easy release of the cargo in acid media and the presence of biotin. On the other hand, the high load capacity of MSN for MB justified its use as cargo, but other compounds with similar redox

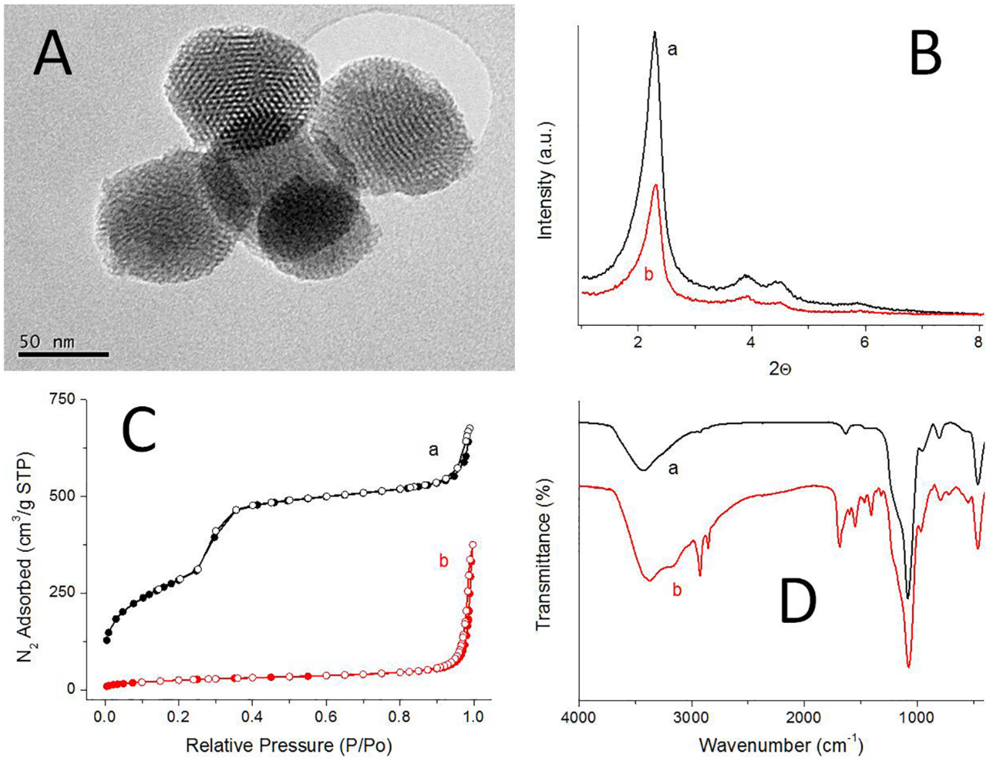

Fig. 2. (A) Representative TEM image of Av/ImB-MSN, (B) Powder X-ray diffraction patterns, (C) N_2 adsorption (closed)/desorption (open) isotherms, and (D) FT-IR spectra for MSN (a) and Av/ImB-MSN (b).

properties and molecular size and geometry could be also employed.

This nanocarrier was characterized by using different techniques. As is illustrated in Fig. 2A, TEM analysis revealed a spherical shape with average diameter of 110 ± 6 nm, and a mesoporous morphology with well-ordered hexagonal pore distribution for Av/ImB-MSN. This MCM-41 type morphology was also confirmed by the characteristics (1 0 0), (1 1 0) and (2 0 0) Bragg reflection peaks in the powder X-ray diffraction spectra (Fig. 2B) [14].

Fig. 2C shows the N_2 adsorption/desorption isotherms of the initial MSN and the Av/ImB-MSN nanocarrier. The starting nanoparticles showed the typical type IV isotherms of mesoporous silica nanomaterials [15], with average pore diameter of 2.2 nm and BET specific surface of 1050 m^2/g. However, encapsulation of MB and construction of the imminobiotin/avidin gate-like ensemble on the nanoparticle surface was confirmed by the characteristic N_2 adsorption/desorption isotherms of mesoporous materials with filled pores, with a reduced BET specific surface of 96 m^2/g and no appreciable porosity. Some N_2 adsorption was observed for the Av/ImB-MSN nanocarrier at high relative pressure values. This fact is attributed to textural porosity.

The nanocarrier also showed the characteristics FT-IR spectra of siliceous materials [12], with adsorption bands at 460 cm^{-1}, 811 cm^{-1}, 954 cm^{-1} and 1077 cm^{-1} ascribed to the Si-O, SiO4, Si-OH and Si-O-Si vibrations, respectively (Fig. 2D). The presence of the adsorption bands at 1550 cm^{-1}, 1687 cm^{-1} and 2840–2920 cm^{-1}, which are ascribed to the N—H, C═O and C—H vibrations, respectively, allows to confirm the Av/ImB ensemble. In addition, total alkaline hydrolysis of Av/ImB-MSN revealed a MB content of 11 mmol/g SiO_2.

The avidin-capped nanocarrier was tested for the on-command controlled release of the encapsulated redox probe at room temperature, by using 4 mM biotin and 200 mM H_2SO_4 as trigger. This assay was performed by measuring the absorbance at 663 nm of the released MB from 9 mg/mL Av/ImB-MSN suspensions in 10 mM sodium phosphate buffer, pH 7.4, in the absence and the presence of the triggers. As can be observed in Fig. 3, only a slight release of MB was noticed in the

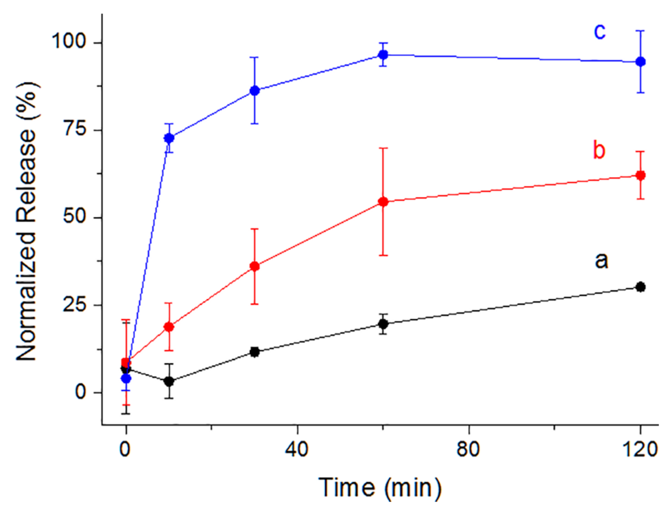

Fig. 3. Kinetics of MB release from Av/ImB-MSN in 10 mM sodium phosphate buffer, pH 7.4, in the absence (a) and the presence of 4 mM biotin (b) and 200 mM H_2SO_4 (c).

absence of the triggers, suggesting that the nanocarrier is still tightly capped. On the contrary, MB was progressively released from the nanocarrier in the presence of biotin, which could be ascribed to the displacement of the imminobiotin residues from its complex with avidin, due to the higher affinity of this protein from biotin [13]. A more pronounced and faster release of MB was observed by incubating Av/ImB-MSN in acid media, due to pH-mediated disruption of the imminobiotin/avidin complex. Accordingly, H_2SO_4 was selected as trigger for electroanalytical experiments.

To demonstrate the application of this nanodevice for biosensing, as a proof-of-concept, an electrochemical aptasensor for CEA was constructed. As illustrated in Fig. 1B, an anti-CEA specific DNA hairpin

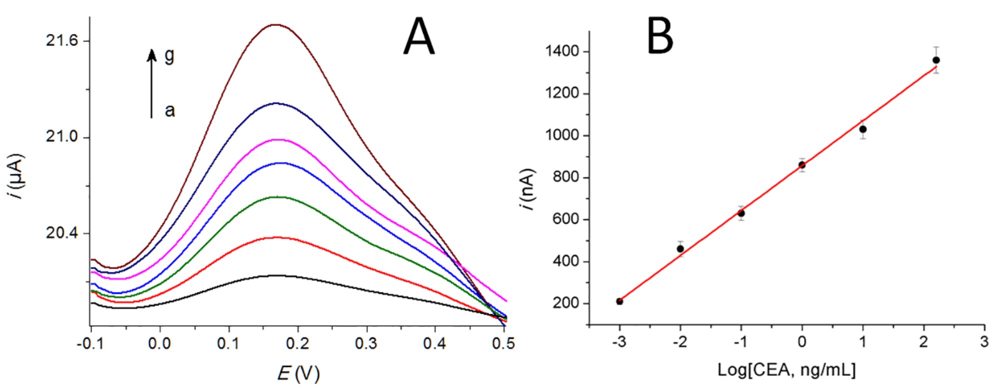

Fig. 4. (A) Differential pulse voltammograms recorded at the Apt/AuNP/SPE electrodes in 0.5 M H_2SO_4 after incubation with 0 ng/mL (a), 1.0 pg/mL (b), 10 pg/mL (c), 100 pg/mL (d), 1.0 ng/mL (e), 10 ng/mL (f) and 160 ng/mL CEA and 0.5 mg/mL Av/ImB-MSN dispersion. (B) Calibration curve for CEA aptasensor in buffered solutions.

aptamer modified with thiol and biotin groups was attached to AuNP/SPE, and the sensing surface was further coated with BSA. We envisioned that the aptamer hairpin conformation unfold upon recognition of CEA, unmasking the biotin residue at the 3́end, allowing further association with the Av/ImB-MSN nanocarrier for signal amplification.

The construction and working conditions for this aptasensor were optimized, by measuring the analytical response toward 2.0 ng/mL CEA. High response was achieved by incubating 7 μM aptamer during 20 min on the electrode surface, and using 2% (w/v) BSA as coating solution. Best performance was also obtained by sequential incubation of the aptansensor with CEA samples and 0.5 mg/mL Av/ImB-MSN dispersion during 20 min. Finally, 0.5 M H_2SO_4 was employed as trigger to release the encapsulated redox probe.

The aptasensor was then evaluated for the determination of CEA. Fig. 4A shows the DPV response of the electrode toward different concentrations of this biomarker. A small analytical signal was obtained for the control solution without CEA. However, a progressive increase in the current intensity was observed by increasing the concentration of the biomarker in the incubation solutions.

As is illustrated in Fig. 4B, the measured current values followed a linear dependence with the logarithm of CEA concentration between 1.0 pg/mL and 160 ng/mL, according to the following equation (r^2 = 0.994, n = 6):

$$i\ (\text{nA}) = 214\cdot\log[\text{CEA}]\ (\text{ng/mL}) + 858$$

The aptasensor was also tested in 5-fold diluted human serum samples by using the standard addition method, showing a linear relationship between the current intensity values and the logarithm of CEA concentration between 1.0 pg/mL and 10 ng/mL. This behaviour was fitted to the following equation (r^2 = 0.989, n = 6):

$$i\ (\text{nA}) = 56\cdot\log[\text{CEA}]\ (\text{ng/mL}) + 60$$

Accordingly, we can conclude that this matrix have a considerable effect on the sensor performance.

It should be highlighted that normal serum concentrations of CEA are lower than 2.5 ng/mL and 5 ng/mL in non-smoking and smoking healthy people, respectively. On the other hand, higher levels can be associated with cancer diseases [16]. Accordingly, this aptasensor is then suitable for CEA detection in clinical samples.

The limit of detection for this biosensor, calculated according to the IUPAC rules [17], was estimated to be 280 fg/mL and 510 fg/mL in buffered solutions and diluted human serum samples, respectively. This parameter was similar or even lower than those previously reported for other electrochemical biosensors for CEA determination [18–20]. The aptasensor also showed good reproducibility with a relative standard deviation of 8.6%, as determined by measuring the analytical response of 10 different electrodes toward 2 ng/mL CEA solution.

4. Conclusions

In this work we described an original signal amplification approach for affinity electrochemical biosensors based on MSN loaded with a redox probe and capped with an avidin/imminobiotin pH-responsive ensemble. This nanocarrier can bind biotin-labeled biomolecules and further release the encapsulated redox probe under demand. As a proof-of-concept, this signal amplification approach was here succesfully validated with an electrochemical aptasensors for CEA, but this strategy can be extended to many other affinity biosensors using biotinylated bioreceptors. In addition, the possibility to tailor design similar nanocarriers with controlled size and load capacity, and by using different redox probes as cargo opens new opportunities to construct highly sensitive electrochemical biosensor devices.

Acknowledgements

Financial support from the Spanish Ministry of Economy and Competitiveness (projects CTQ2014-58989-P, CTQ2015-71936-REDT, CTQ2017-87954-P and RTI2018-100910-B-C41, fellowship BES-2015-073565 to SJF) and the Generalitat Valencia (Project PROMETEO/2018/024) are gratefully acknowledged.

References

[1] J. Lei, H. Ju, Chem. Soc. Rev. 41 (2012) 2122.
[2] L. Ding, A.M. Bond, J. Zhai, J. Zhang, Anal. Chim. Acta 797 (2013) 1.
[3] M. Zouari, S. Campuzano, J.M. Pingarrón, N. Raouafi, Biosens. Bioelectron. 91 (2017) 40.
[4] M. Zouari, S. Campuzano, J.M. Pingarrón, N. Raouafi, Electrochim. Acta 262 (2018) 39.
[5] B. Borisova, M.L. Villalonga, M. Arévalo-Villena, A. Boujakhrout, A. Sánchez, C. Parrado, J.M. Pingarrón, A. Briones-Pérez, R. Villalonga, Anal. Bioanal. Chem. 409 (2017) 5667.
[6] S. Liu, Z. Yang, Y. Chang, Y. Chai, R. Yuan, Biosens. Bioelectron. 119 (2018) 170.
[7] Y.X. Chen, K.J. Huang, K.X. Niu, Biosens. Bioelectron. 99 (2018) 612.
[8] G. Liu, Y. Lin, Talanta 74 (2007) 308.
[9] E. Aznar, M. Oroval, L. Pascual, J.R. Murguía, R. Martinez-Manez, F. Sancenon, Chem. Rev. 116 (2016) 561.
[10] Q. Meng, S. Shi, C. Liang, D. Liang, W. Xu, S. Ji, B. Zhang, Q. Ni, J. Xu, X. Yu, Onco Targets Ther. 10 (2017) 4591.
[11] C. Ma, H. Liu, L. Zhang, H. Li, M. Yan, X. Song, J. Yu, Biosens. Bioelectron. 99 (2018) 8.
[12] P. Díez, A. Sánchez, C. Torre, M. Gamella, P. Martínez-Ruíz, E. Aznar, R. Martínez-Máñez, J.M. Pingarrón, R. Villalonga, ACS Appl. Mat. Interfaces 8 (2016) 7657.
[13] H. Inoue, K. Sato, J.I. Anzai, Biomacromolecules 6 (2005) 27.
[14] M. Kruk, M. Jaroniec, J.M. Kim, R. Ryoo, Langmuir 15 (1999) 5279.
[15] R. Villalonga, P. Díez, A. Sánchez, E. Aznar, R. Martínez-Máñez, J.M. Pingarrón, Chem. Eur. J. 19 (2013) 7889.
[16] G.A. Rivas, M.C. Rodríguez, M.D. Rubianes, F.A. Gutierrez, M. Eguílaz, P.R. Dalmasso, E.N. Primo, C. Tettamanti, M.L. Ramírez, A. Montemerlo, P. Gallay, C. Parrado, Appl. Mater. Today 9 (2017) 566.
[17] H.P. Loock, P.D. Wentzell, Sens. Actuators B Chem. 173 (2012) 157.
[18] G. Paniagua, A. Villalonga, M. Eguílaz, B. Vegas, C. Parrado, G. Rivas, P. Díez, R. Villalonga, Anal. Chim. Acta 1061 (2019) 84.
[19] Z. Hong, G. Chen, S. Yu, R. Huang, C. Fan, Anal. Meth. 10 (2018) 5364.
[20] J. Huang, J. Tian, Y. Zhao, S. Zhao, Sens. Actuators B Chem. 206 (2015) 570.